

---

# HIDDEN DEFECT CHEMISTRY IN ION-IRRADIATED $\text{MoS}_2$ FIELD-EFFECT TRANSISTORS REVEALED BY PHOTOCURRENT LOSS

---

**Leon Daniel**

Faculty of Physics and CENIDE  
University of Duisburg-Essen  
Duisburg

**Dedi Sutarma**

Faculty of Physics and CENIDE  
University of Duisburg-Essen  
Duisburg

**Leon Klieve**

Faculty of Physics and CENIDE  
University of Duisburg-Essen  
Duisburg

**Osamah Kharsah**

Faculty of Physics and CENIDE  
University of Duisburg-Essen  
Duisburg

**Ulrich Hagemann**

ICAN and CENIDE  
University of Duisburg-Essen  
Duisburg

**Oliver Altenhoff**

Faculty of Physics and CENIDE  
University of Duisburg-Essen  
Duisburg

**Stephan Slezione**

Faculty of Physics and CENIDE  
University of Duisburg-Essen  
Duisburg

**Lars Breuer**

Faculty of Physics and CENIDE  
University of Duisburg-Essen  
Duisburg

**Peter Kratzer**

Faculty of Physics and CENIDE  
University of Duisburg-Essen  
Duisburg

**Marika Schleberger\***

Faculty of Physics and CENIDE  
University of Duisburg-Essen  
Duisburg  
marika.schleberger@uni-due.de

## ABSTRACT

Defect engineering in monolayer  $\text{MoS}_2$  is a promising route to tune field-effect transistors (FETs), but the electronic response of defects in processed devices can be masked by contacts, substrate effects, adsorbates, and chemical passivation. Here, we irradiate  $\text{MoS}_2$  FETs with low-energy 40 eV  $\text{Ar}^+$  ions to preferentially create sulfur vacancies ( $V_S$ ) in the channel while minimizing substrate damage. We compare dark and illuminated electrical characterization with surface analysis and first-principles calculations. Dark transfer characteristics show an apparent robustness against irradiation up to moderate fluences, with pronounced degradation only at the highest fluence. Under 532 nm illumination, however, the photocurrent and light-induced photodoping decrease systematically with increasing ion fluence, revealing irradiation-induced changes that are hidden in standard dark measurements. Atomic force microscopy and X-ray photoelectron spectroscopy show substantial carbon-containing residues on processed devices even after extended cleaning. We propose that such residues may provide a reservoir for hydrocarbon-mediated passivation of sulfur vacancies. Density-functional-theory calculations provide a microscopic model consistent with this scenario: unsaturated  $V_S$  introduce in-gap states,  $\text{H-C}_S$  configurations suppress these states, and carbon substitution without hydrogen leaves defect states in the band gap. Our results highlight carbon-containing surface contamination as a key factor in interpreting defect engineering experiments on  $\text{MoS}_2$  and related TMDC devices.

**Keywords**  $\text{MoS}_2$ , field-effect-transistor, hydrocarbon passivation, defect engineering, density functional theory

## 1 Introduction

Defect engineering is a central strategy for tailoring the electronic and optoelectronic properties of two-dimensional transition-metal dichalcogenides (TMDCs) [1, 2, 3, 4, 5]. In MoS<sub>2</sub>, sulfur vacancies are among the most relevant point defects because they can introduce in-gap states, modify the carrier density, and act as scattering or trapping centers [4, 6]. Such vacancies may arise during growth, processing, plasma exposure, electron irradiation, or ion irradiation. However, the electronic signature of these defects in processed field-effect transistors (FETs) is not necessarily straightforward. Contacts, adsorbates, substrate-induced charge trapping, and fabrication residues can strongly affect the measured transfer characteristics [2, 7]. In addition, chemically active vacancy sites may react with residual species from the sample surface or environment, thereby masking their expected electronic impact [8].

Monolayer MoS<sub>2</sub> is a key model system for studying this problem because it combines a direct optical band gap with compatibility with field-effect transistor geometries [9, 10]. Its high surface-to-volume ratio and pronounced optoelectronic response make its transport properties sensitive to light, adsorbates, and the dielectric environment [11, 7, 12]. Device parameters such as doping, memory behavior, carrier mobility, and contact resistance can therefore vary strongly between processed devices and must be considered when interpreting defect-induced changes. Previous studies have shown that MoS<sub>2</sub>-based devices can be modified by electron irradiation, ion irradiation, chemical treatments, and surface adsorbates [1, 2, 3, 4, 5], but the resulting device response often reflects a combination of intrinsic defects, extrinsic residues, and interface effects.

Several reports indicate that MoS<sub>2</sub> FETs can display an unexpectedly weak or non-monotonic degradation of their dark electrical characteristics after ion irradiation [8, 13]. Such apparent robustness may originate from substrate-related effects, contact modifications, or chemical passivation of irradiation-induced defects. In particular, it has been suggested that chemically active sulfur vacancies may react with sputtered or residual species, thereby masking the direct impact of irradiation on the channel [8]. More generally, this raises the question whether defect-rich MoS<sub>2</sub> devices necessarily reveal their defect density in standard dark electrical measurements, or whether chemically passivated defects can remain electronically hidden.

In this work, we use low-energy Ar<sup>+</sup> irradiation as a controlled route to introduce sulfur vacancies into MoS<sub>2</sub> FETs. The ion energy is chosen to preferentially create near-surface defects in the MoS<sub>2</sub> channel while minimizing damage to the substrate and contacts. The dark transfer characteristics suggest an apparent robustness against irradiation up to moderate fluences, with pronounced degradation only at the highest fluence. In contrast, measurements under 532 nm illumination reveal a systematic reduction of the photoresponse with increasing ion fluence. This discrepancy shows that the defect response is conditional and can be overlooked when only dark electrical characteristics are considered.

We examine whether this apparent defect saturation can be explained by carbon-containing surface residues. Carbon contamination is common in processed and synthetic TMDC samples and may originate from growth precursors, ambient exposure, or lithographic processing [14, 15, 16, 17, 18, 19, 20]. In our processed MoS<sub>2</sub> devices, surface analysis reveals substantial carbon-containing residues, including hydrocarbon-like components. Such residues provide a plausible reservoir of carbon-containing fragments that may interact with sulfur vacancies generated during ion irradiation.

This scenario is motivated by recent atomic-scale studies of carbon-related defects in TMDCs. In WS<sub>2</sub> and WSe<sub>2</sub>, carbon-hydrogen (CH) impurities have been identified as persistent unintentional defects, and CH incorporation at chalcogen sites has been shown to be energetically favorable [14, 15, 16]. In WS<sub>2</sub>, a CH complex at a chalcogen vacancy yields a binding energy of  $-0.55$  eV [15]. Moreover, CH produces less lattice strain than C, CH<sub>2</sub>, or CH<sub>3</sub> configurations [18]. Although these results were obtained mainly for WS<sub>2</sub> and WSe<sub>2</sub>, they establish CH substitution at chalcogen sites as a chemically plausible motif in TMDCs.

Based on these considerations, we propose hydrocarbon-mediated passivation of sulfur vacancies as a plausible microscopic scenario. In particular, H-C<sub>S</sub> configurations provide a model system for understanding how vacancy-related in-gap states could be suppressed, thereby masking the effect of defects in dark transfer measurements. The observed degradation under illumination then suggests that the chemical or electronic state of these passivated defects may be modified by light. We support this interpretation by combining dark and illuminated electrical measurements with surface analysis and density-functional-theory calculations.

## 2 Results and Discussion

We begin by establishing the baseline properties of the MoS<sub>2</sub> FET prior to ion irradiation. An optical micrograph of the device is shown in Figure 1(a). The monolayer MoS<sub>2</sub> was grown by chemical vapor deposition (CVD) directly on p-doped SiO<sub>2</sub>/Si wafers.

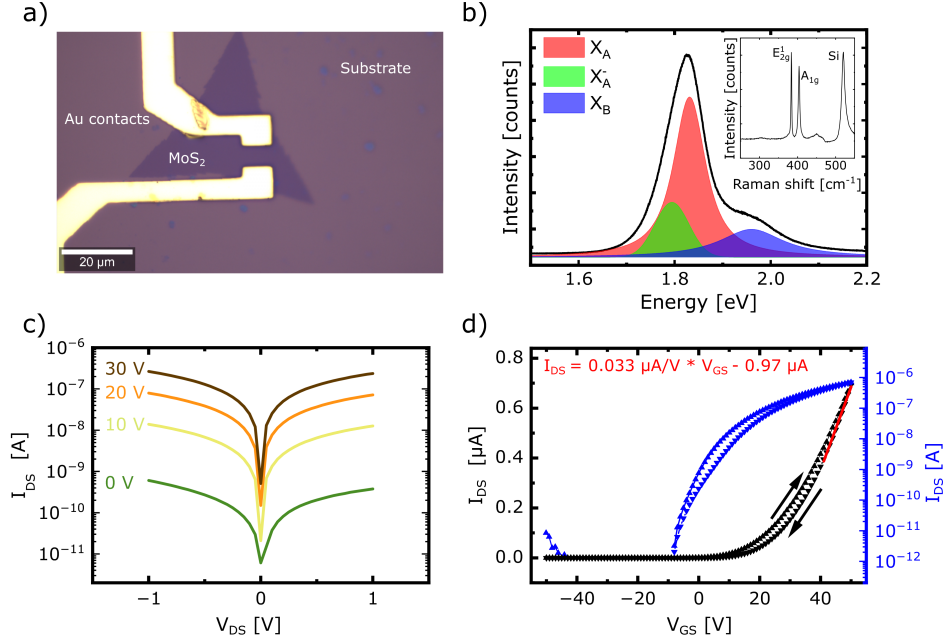


Figure 1: (a) Microscopic image of an MoS<sub>2</sub> monolayer with Cr/Au contacts on a SiO<sub>2</sub> substrate. (b) PL spectrum of MoS<sub>2</sub> confirming the monolayer properties of the flake. The insert shows the corresponding Raman spectra. (c) Output characteristics of an MoS<sub>2</sub> FET. The output current for negative and positive V<sub>DS</sub> applied is rather symmetric, with a ratio of  $\approx 1.1$ , indicating mostly ohmic behavior. (d) Transfer characteristics of an MoS<sub>2</sub> FET with linear and logarithmic y-axis. The backswep measurement is linearly fitted for a range from 40 V to 50 V for extracting the threshold voltage and carrier mobility.

As a first characterization step, we confirm the monolayer character of the MoS<sub>2</sub> flake by photoluminescence and Raman spectroscopy, as shown in Figure 1(b). The photoluminescence spectrum exhibits the characteristic emission features of monolayer MoS<sub>2</sub>, associated with excitonic recombination processes [9, 21, 22]. In addition, the A exciton peak shows asymmetric properties with a low-energy tail, consistent with the presence of trions and thus with electron doping of the monolayer. [23]. The Raman signal is consistent with as-grown monolayer MoS<sub>2</sub>, with the A<sub>1g</sub> and E<sub>2g</sub> modes separated by approximately 20 cm<sup>-1</sup> [22].

The as-grown flake was subsequently processed into a FET by defining Cr/Au source and drain contacts using standard photolithography. The Cr layer serves as the adhesion layer and forms the direct contact to MoS<sub>2</sub>, while Au provides the highly conductive top electrode. Cr has been proposed as a favorable contact metal for MoS<sub>2</sub> because of its suitable work function and high density of states near the Fermi level [24, 25]. Nevertheless, the contact properties of processed MoS<sub>2</sub> FETs can be strongly affected by interface contamination, oxidation, or lithographic residues, which may introduce additional barriers and increase the contact resistance [25]. The degenerately doped Si substrate was used as a global back gate.

Lithographic processing can leave residual organic material on the MoS<sub>2</sub> surface. To assess this contribution, we investigated a processed MoS<sub>2</sub> reference sample by atomic force microscopy (AFM). After a standard lift-off process, the surface remains covered by nanoscale residues, visible as protrusions in the AFM topography. Repeated acetone cleaning (3×4 h) substantially reduces the surface roughness from 1.9 nm to 0.3 nm. However, residual material can still accumulate near the Au contacts, indicating that the fabrication process does not fully remove surface contamination. As discussed below, XPS confirms that these residues contain substantial carbon.

Electrical measurements are done for further characterization of the sample. For all electrical measurements, the device is placed under high vacuum ( $\leq 5 \cdot 10^{-5}$  mbar) to minimize the influence of adsorbates and influence of the atmosphere. The Cr/Au contacts act as drain and source contacts, enabling the performance of output measurements, where the drain-source current (I<sub>DS</sub>) is measured in dependence of the drain-source voltage (V<sub>DS</sub>). The output characteristic of the sample is shown in Figure 1(c). V<sub>DS</sub> is swept from -1 V to 1 V and back, with the measurement sweep backwards being displayed. The measurements were repeated for different voltages, measured relative to the potential at the source contact, applied at the gate (V<sub>GS</sub>). The nearly symmetric output characteristics provide little evidence for a dominant rectifying Schottky barrier and indicate predominantly ohmic behavior in the measured voltage range [26, 27, 2].

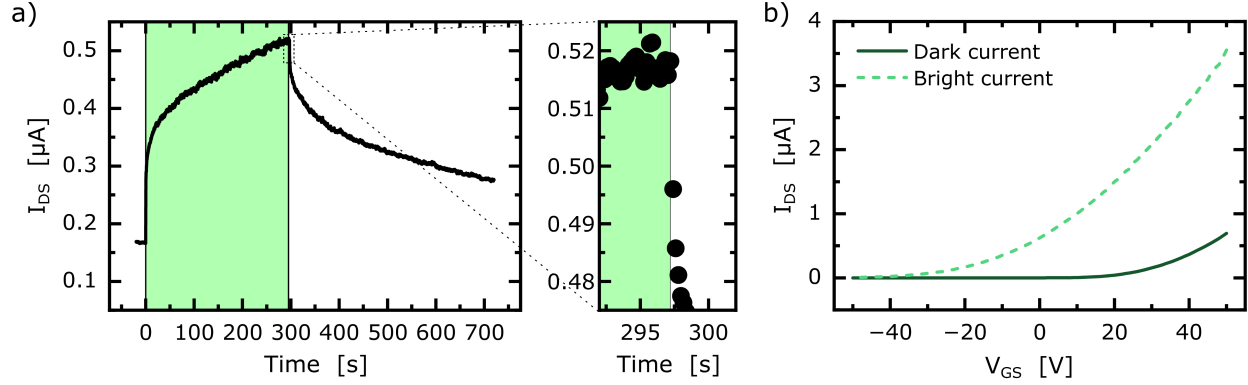


Figure 2: (a) Time-resolved photocurrent measurements for MoS<sub>2</sub>. The channel is illuminated for around 300 s with a 532 nm laser. The duration of the illumination is marked in the figure. A zoomed-in look at the data shows that the current changes only minimally immediately (200 ms) after the laser is turned off compared to the total current induced by the laser, indicating that direct photoexcitation is not the dominant contribution to the persistent photocurrent on the observed timescale. (b) Transfer characteristic for an MoS<sub>2</sub> FET under dark and under bright conditions through laser illumination. A shift of the transfer curve to the left indicates how the laser effectively n-dopes the material.

For the transfer measurements,  $V_{DS}$  is held constant at 0.5 V with the  $V_{GS}$  twice swept from -50 V to 50 V back to -50 V in 1 V steps. After the gate voltage is changed, a delay time of 3.6 s is kept, before the output signal by the picoammeter is integrated for 25 ms. These gate-dependent measurements, shown in Figure 1(d), indicate pronounced n-type doping, as commonly observed for MoS<sub>2</sub> FETs [11, 28, 7, 12, 3, 4]. The device shows clear on-off behavior above  $10^3$ , typical for our devices [3]. A possible contribution to this n-type behaviour is carbon incorporation during growth [19], potentially through the precursor used in CVD-growth. Other descriptors introduced in this work, such as carrier mobility  $\mu$  or doping  $n$ , refer to electrons as the majority charge carriers.

The device displays a typical hysteresis effect commonly observed in MoS<sub>2</sub> FETs [12, 29]. Different mechanisms are discussed as the origin of the hysteresis. Fast recombination through intrinsic in-gap states is unlikely to explain the slow hysteresis observed here, as such processes typically occur on ultrafast timescales ( $\leq 10$  ns) [30, 31, 32]. It was shown that the atmospheric environment can impact the hysteresis [33]. As our device operates under vacuum conditions, charge trapping at the interface and in the oxide seems to be the most likely mechanism [12, 34, 35, 36, 37], with the gate voltage pushing electrons in and out of these states over time. This process happens in the order of several minutes, which also holds true in our device, as can be seen in time-resolved gate-dependent measurements (See SI).

The effective mobility is determined through linear fitting the transfer curve for a fixed range at high voltages (Figure 1(d)) through the following expression:

$$\mu = \frac{\delta I_{DS}}{\delta V_{GS}} \frac{1}{C_{ox}} \frac{L}{V_{DS} W} \quad (1)$$

$W$  and  $L$  are the width and length of the conductive channel, with  $C_{ox} = 1.21 \times 10^{-8}$  F/cm<sup>2</sup> being the capacitance per unit area of the oxide [3]. We estimate the mobility of the device to be around 4.3 cm<sup>2</sup>/V·s, typical for such devices [7, 12, 3, 38, 39, 40]. The effective mobility  $\mu$  in the channel material is connected with the mobility of free electrons  $\mu_0$  in the conduction band, the overall electron concentration  $n$ , and the concentration of electrons in extended states  $n_{band}$  with  $\mu = \mu_0 \frac{\delta n_{band}}{\delta n}$  [41, 42]. Electrons in extended states refer to electrons that contribute to band transport. Carrier trapping results in a reduction of the effective mobility.

The extracted mobility is well below the room-temperature phonon-limited value of approximately 150 cm<sup>2</sup>/V·s reported for MoS<sub>2</sub> [41, 43, 44]. This indicates that additional scattering and trapping mechanisms contribute substantially in the processed device [40, 41, 39, 42].

The optoelectronic response of the device was characterized by illuminating the MoS<sub>2</sub> channel with a 532 nm cw laser at a total power of 0.1 mW. As shown in Figure 2(a), illumination leads to a pronounced increase in the drain-source current. The current rises gradually after an initial jump and does not immediately return to its original value after the light is switched off, which is typical for persistent photoconductivity in MoS<sub>2</sub> FETs [7, 45]. The transient response requires at least two characteristic timescales to describe, with  $\tau_1 \approx 15$  s and a slower component  $\tau_2$  exceeding the observed time window [7].

Different processes contribute to the photocurrent, including the direct photoexcitation, desorption of p-doping adsorbates and trapping of carriers [7]. Due to the short lifetime of photogenerated carriers, direct photoexcitation is expected to contribute mainly to the fast component of the photocurrent and is unlikely to dominate the persistent response observed here [7, 31, 30]. This can be seen in Figure 2(a), where the current changes only slightly (20 nA) 200 ms after the laser is turned off, compared to the overall current induced by the laser in the presented measurement. We therefore attribute the persistent photocurrent primarily to slow processes such as desorption of p-doping adsorbates and charge trapping. In Figure 2(b) the effective doping through the laser can be observed through a shift of the transfer curve to the left. For a better overview, we only plot the current for the measurements swept backwards.

The photodoping density is estimated from the light-induced shift of the threshold voltage  $V_{th}$ . For both dark and illuminated transfer curves,  $V_{th}$  is obtained from the intersection of a linear fit with the gate-voltage axis, as illustrated in Figure 1(d). The corresponding photodoping density is calculated as  $n_{ph} = C_{ox} \times \frac{V_{th}(\text{Dark}) - V_{th}(\text{Bright})}{e}$  [46]. For the measurements shown, we see a strong increase in n-doping of about  $1.8 \times 10^{12}$  1/cm<sup>2</sup> induced by the laser.

Low-energy Ar<sup>+</sup> irradiation is used to introduce defects into the MoS<sub>2</sub> channel. The ion energy is set to 40 eV, where near-surface defect creation in MoS<sub>2</sub> is favored while substrate sputtering and the formation of deep oxide defects are expected to be strongly reduced [47, 48]. In this regime, sulfur vacancies are expected to be the dominant irradiation-induced defects, with a high probability of vacancy creation per incident Ar<sup>+</sup> ion [49].

For irradiation the sample is taken out of the analysis chamber and placed into an ultra-high vacuum (UHV) chamber equipped with an ion sputter gun. During this transfer process the sample is exposed to ambient conditions for a short period of about 5 minutes. Before conducting the ion irradiation, the sample is left to rest under UHV conditions (10<sup>-8</sup> mbar) for at least 12 hours to reduce weakly bound atmospheric adsorbates. After each irradiation step, the sample is taken out of the UHV and placed back into the analysis chamber, where the sample is again characterized. The corresponding transfer curves under dark conditions are shown in Figure 3(a).

For each fluence, the mobility is determined. Additionally, changes in doping relative to the initial device state before irradiation are determined similarly as the photodoping with:

$$\Delta n_D = C_{ox} \times \frac{\Delta V_{th}}{e} \quad (2)$$

We note that charge accumulation on the oxide surface can lead to oxide breakdown at higher irradiation fluences. In the device shown here, a significant gate-source leakage current appears after an irradiation fluence of  $6 \times 10^{13}$  cm<sup>-2</sup> for gate voltages above 10 V. The measured drain-source current was therefore corrected by subtracting the measured leakage current.

If unsaturated sulfur vacancies dominated the electronic response, one would expect a decrease in current and mobility already at low to moderate fluences. Instead, the current remains nearly unchanged during the first three irradiation steps (Figure 3(b)). This is also seen in the mobility and doping (See SI). Only at a high fluence a strong decrease in the current can be observed. This behavior was observed in two reference samples, where the transfer characteristic stays constant with several irradiation steps only to significantly reduce for high fluences (see Supporting Information and [50]).

Fekri *et al.* reported a related non-monotonic response in MoS<sub>2</sub> FETs irradiated with 5 keV and 7.5 keV He<sup>+</sup> as well as 7.5 keV Ne<sup>+</sup> ions. They attributed the increased conductivity at low and intermediate fluences to charges implanted in the oxide, which effectively act as an additional gate [8]. Only at higher fluences does the ion irradiation lead to the current being reduced.

This mechanism would be expected to modify the hysteresis, since long-lived oxide or interface traps contribute to the memory window of MoS<sub>2</sub> FETs. We therefore extract the memory window from the forward and backward gate sweeps for each irradiation step (Figure 3(c)). Defects created in the oxide increase the hysteresis by acting as long-time charge traps [51]. We observe limited change in the memory properties of the used MoS<sub>2</sub> FET. After the first irradiation step an increase in the hysteresis width of around 25% can be seen, which remains constant for the next two irradiation steps and decreases for higher irradiation steps. In a previous study, we irradiated MoS<sub>2</sub> with fast (180 keV) highly charged Xe<sup>30+</sup> ions, depositing energy deep in the oxide, led to a consistent increase in the memory window in contrast to the measurements presented in this work [3]. This indicates that the irradiation does not lead to a pronounced increase in long-lived oxide or interface traps that would dominate the hysteresis response.

The transfer measurements were then repeated under illumination with a 532 nm laser, as shown in Figure 3(d). Compared with the dark measurements, the illuminated transfer curves show a markedly different fluence dependence. Already at low fluences the drain-source current decreases under illumination (Figure 3(e)), accompanied by a significant reduction in photo-doping (Figure 3(f)).

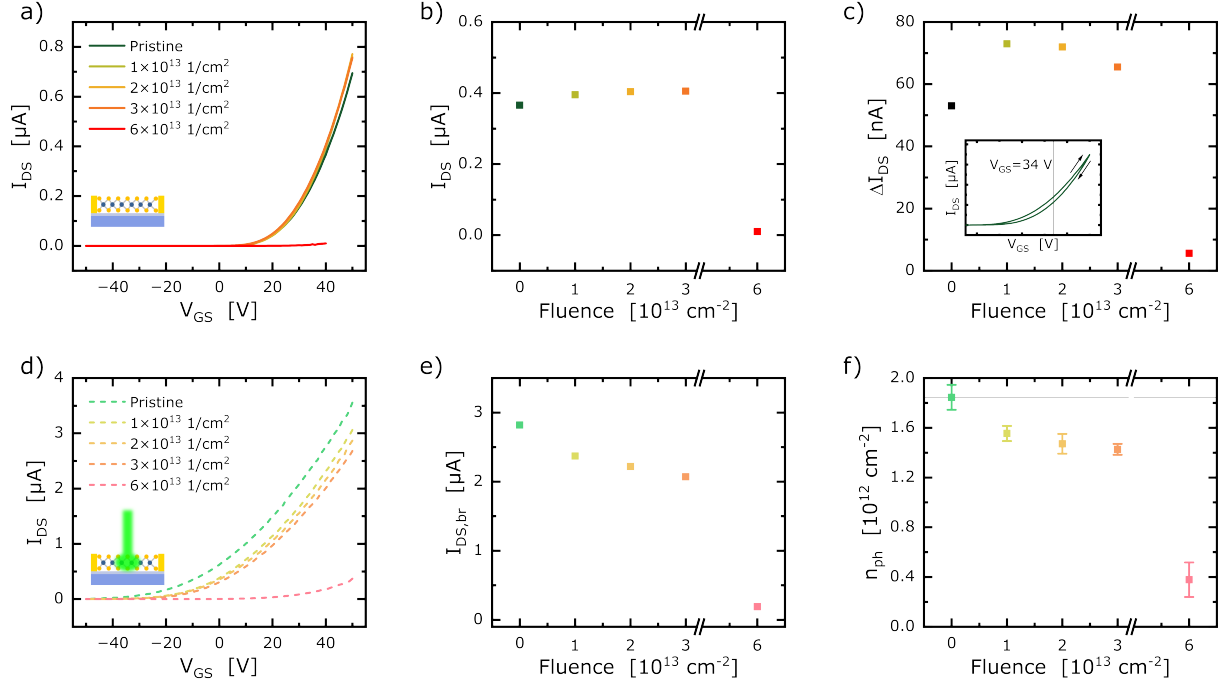


Figure 3: (a) Transfer curve for an MoS<sub>2</sub> FET under dark conditions for different fluences of Ar<sup>+</sup> ions. Through fitting the transfer curve at high voltages, the mobility and threshold voltage are extracted. (b)  $I_{DS}$  extracted from (a) at  $V_{GS}=40$  V. The current remains nearly unchanged up to a fluence of  $3 \times 10^{13}$  ions/cm<sup>2</sup> and only decreases for high fluences. (c) Memory window extracted from the hysteresis for each irradiation step. The memory window was measured at a gate voltage of  $V_{GS}=34$  V as indicated in the insert, where the memory window is the widest for this device. The limited changes suggest that ion-induced oxide trapping is not the dominant contribution under these irradiation conditions. (d) Transfer curve for an MoS<sub>2</sub> FET under 532 nm illumination for different irradiation steps. (e)  $I_{DS}$  extracted from (d) at a gate voltage of 40 V. In contrast to the measurements under dark conditions, the current decreases with each irradiation step. (f) Photo doping, additional carriers induced by the laser, for each irradiation step.

The measurements under illumination and under dark conditions show seemingly contradictory results. The comparison between dark and illuminated measurements suggests that irradiation-induced changes can be hidden under dark measurement conditions.

If the irradiation-induced sulfur vacancies remained electronically active and unsaturated, they would be expected to introduce localized in-gap states. These states do not necessarily act as shallow reversible traps, but they can still affect transport by localizing charge, modifying the apparent carrier density, promoting recombination under illumination, or increasing charged-defect scattering [4]. The weak changes observed in the dark transfer characteristics are therefore difficult to reconcile with a large population of electronically active, unsaturated sulfur vacancies alone.

A plausible explanation for this apparent masking is an initial chemical passivation of the sulfur vacancy sites. One possible passivation pathway is oxygen incorporation into sulfur vacancies, with oxygen supplied either by substrate sputtering [8] or by atmospheric exposure during sample transfer. Oxygen is known to occupy V<sub>S</sub> sites in TMDCs and can form relatively inert substitutional defects [52, 53]. Once atomic oxygen is incorporated into a sulfur vacancy, its removal is expected to be energetically unfavorable, as the formation energy to remove substitutional oxygen exceeds that of sulfur removal from the MoS<sub>2</sub> lattice [54, 6]. Oxygen substitution of irradiation-induced vacancies is therefore unlikely to fully account for the observed behavior.

This argument is strengthened when we consider two possible oxygen sources. First, SRIM calculations indicate that, at the ion energy used here, substrate sputtering is negligible. Substrate-derived oxygen species are therefore unlikely to provide a dominant source for oxygen passivation. This is in accordance with the limited change in the memory window, which suggests that long-lived oxide or interface traps do not dominate the irradiation response. Secondly, passivation of V<sub>S</sub> sites by incorporating atmospheric oxygen is expected to be kinetically limited under ambient conditions, with

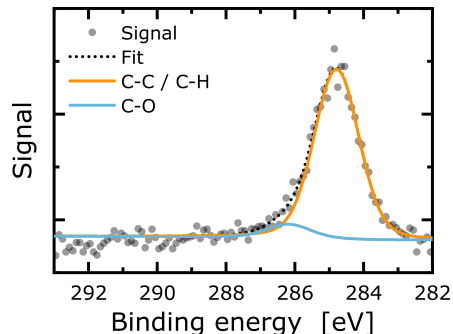


Figure 4: XPS spectrum of the C 1s region measured on a processed MoS<sub>2</sub> reference sample after cleaning. The spectrum is consistent with hydrocarbon-like residues and partially oxidized carbon species. C-C and C-H bonds contribute to  $\approx 90\%$  and C-O bond  $\approx 10\%$  to the signal.

reported timescales on the order of days due to the activation barrier for chemisorption [55]. We therefore consider oxygen-based passivation unlikely to dominate on the relevant experimental timescale.

Alternatively, we propose that carbon-related defect formation should be considered. Recent studies have shown that TMDCs frequently exhibit carbon contamination [14, 15, 16, 17, 18, 19, 20]. Carbon-containing precursors, such as sodium cholate used in this study, are commonly used during growth. Subsequent device fabrication also exposes the material to additional organic species, i.e. photoresist material. X-ray photoelectron spectroscopy (XPS) analysis of a processed MoS<sub>2</sub> reference sample after cleaning reveals substantial carbon-containing surface contamination (Figure 4 and SI). The C 1s spectrum contains a dominant low-binding-energy carbon component, contributing to  $\approx 90\%$  of the carbon-related signal, commonly assigned to C-C/C-H environments, together with a higher-binding-energy C-O contribution, contributing to  $\approx 10\%$  of the carbon-related signal. This is consistent with hydrocarbon-like residues and partially oxidized organic contamination.

In light of this, previous studies have also reported alkane-covered TMDC surfaces under ambient conditions [56]. Therefore, we argue that such surface contamination represents a readily available reservoir of carbon-containing species, whose role in irradiated TMDC-based FETs may be overlooked.

These contaminants may interact with sulfur vacancies generated during ion irradiation. In addition, ion bombardment can fragment surface hydrocarbons and thereby create reactive hydrocarbon fragments and radicals [57]. We therefore hypothesize that ion-induced sulfur vacancies is highly susceptible to passivation by carbon-containing fragments derived primarily from residual surface organics. Additional contributions from hydrocarbon background species in the vacuum system or from ambient exposure during sample transfer cannot be excluded.

The resulting carbon-related vacancy complexes are expected to differ from substitutional oxygen defects. Oxygen incorporation can fully saturate the sulfur vacancy and form a comparatively stable O<sub>S</sub> configuration. Carbon incorporation, by contrast, may leave the defect site chemically or electronically unsaturated unless additional moiety are involved. In related TMDC systems, this H-C<sub>S</sub> configuration has been identified as energetically favorable carbon-related defects [14, 15, 16, 17, 18]. Deliberate introduction of H-C<sub>S</sub> in WS<sub>2</sub> FETs produced transport trends that are qualitatively similar to our dark measurements, including an initial increase in current followed by degradation at higher concentrations [18]. Although the host material and doping response differ, these results demonstrate that H-C<sub>S</sub> defects can substantially modify the transport properties of TMDC FETs. This makes H-C<sub>S</sub> a plausible microscopic model for carbon-mediated vacancy passivation in the present MoS<sub>2</sub> devices.

Accordingly, we suggest that carbon-mediated passivation can suppress vacancy-related in-gap states under dark conditions, while illumination may modify the electronic or chemical state of these passivated defects, and thereby reveal the irradiation-induced changes in the photoresponse.

To further corroborate our hypothesis, we have modeled the occupation of a V<sub>S</sub> site by C<sub>S</sub> and H-C<sub>S</sub> via DFT calculations (For details see Method section). In Figure 5(a)-(d) we show the band structure of pristine MoS<sub>2</sub>, with a sulfur vacancy, and the described modification. The presence of a sulfur vacancy induces three gap states (Figure 5(b)) coming predominantly from the Mo-d orbital: one occupied bonding level, located just above the valence band, and a pair of energy-equivalent, unoccupied antibonding levels (purple). The H-C<sub>S</sub> addition effectively saturates the dangling bonds of Mo (Figure 5(c)), removing mid-gap states that can act as trapping centers. As no new carrier traps are introduced, this provides a plausible microscopic model for the absence of strong dark-current degradation in our measurements.

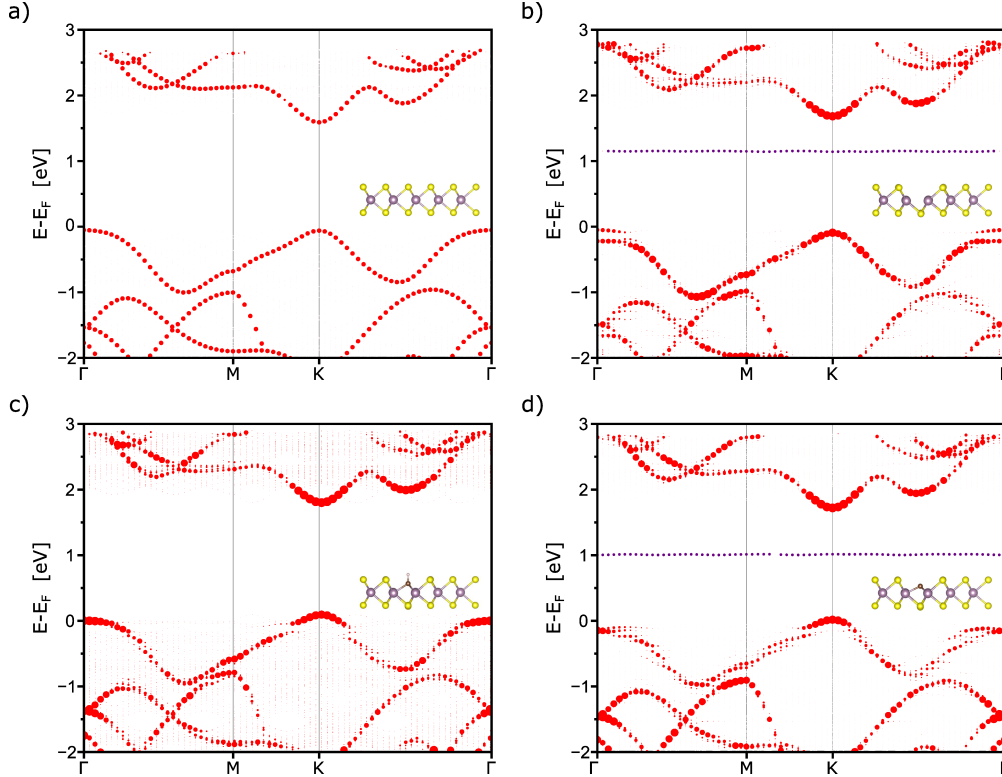


Figure 5: Unfolded band structures from monolayer MoS<sub>2</sub>  $5 \times 5$  supercell, pristine (a), sulfur vacancy ( $V_S$ ) (b), CH substitution (H- $C_S$ ) on sulfur vacancy (c), carbon occupying sulfur vacancy ( $C_S$ ) (d). Typical in-gap states stemming from  $V_S$  are saturated with CH substitution.

To assess the thermodynamic stability of the defect configurations, we calculated their respective formation energies. The formation energy ( $E_f$ ) for a pristine sulfur vacancy ( $V_S$ ) was determined to be 3.01 eV. In comparison, the formation of H- $C_S$  yielded an  $E_f$  of 2.76 eV. Using the  $V_S$  configuration as a reference, the incorporation of the H-C group into the vacancy site is exothermic by  $-0.25$  eV, indicating that the plugging process is energetically favorable.

Band structure calculation on Figure 5(d) shows that carbon occupation alone fails to fully saturate  $V_S$  sites, leaving behind an in-gap state. Defect states reduce the population of mobile carriers in the conduction band while increasing the number of trapped carriers that do not participate in charge transport, thereby lowering the effective mobility [4, 41, 42]. To evaluate whether H- $C_S$  should be regarded as an inert passivation configuration, we calculate the reaction enthalpy  $\Delta H$  (at zero temperature and pressure) for the reaction  $H-C_S \rightarrow C_S + \frac{1}{2}H_2 + \Delta H$  where  $\Delta H$  was computed to be  $-1.1$  eV. We suggest that H- $C_S$  formation at  $V_S$  sites passivates vacancy-related gap states and thereby masks the effects of ion irradiation at low fluences in TMDC devices. The calculated reaction enthalpy indicates that dehydrogenated  $C_S$ -like configurations are energetically accessible from H- $C_S$ , suggesting that these carbon-related defect configurations may be less inert than oxygen-passivated vacancies. Such configurational or electronic changes could contribute to the observed light-induced degradation of the photoresponse.

### 3 Conclusions

We show that processed MoS<sub>2</sub> FETs can appear robust against low-energy ion irradiation when characterized under dark conditions. While the dark transfer characteristics remain nearly unchanged up to moderate fluences, photocurrent measurements reveal a systematic degradation with increasing ion fluence. This demonstrates that irradiation-induced changes can be hidden in standard electrical characterization and become apparent only under illumination.

We propose carbon-mediated passivation of sulfur vacancies as a plausible explanation for this behavior. XPS analysis reveals a significant carbon species contamination on processed MoS<sub>2</sub> devices, providing a potential reservoir for hydrocarbon-derived fragments.

Density functional theory (DFT) calculations yield a microscopic framework that aligns with this proposed mechanism: H-C<sub>s</sub> configurations suppress vacancy-related in-gap states, whereas carbon substitution without hydrogen leaves defect states in the band gap. The different behavior under dark and illuminated conditions suggests that illumination may modify the chemical or electronic state of such passivated defects, revealing irradiation-induced changes in the photoresponse. These findings underline the importance of carbon-containing surface contamination and light-dependent characterization for interpreting defect engineering in MoS<sub>2</sub> and related TMDC devices.

## 4 Methods

### 4.1 Sample Preparation

Sample preparation followed a standard recipe [3]. For the CVD process, 2% aqueous sodium cholate were spin-coated onto cleaned Si/SiO<sub>2</sub> substrates as seeding promoters. Ammonium heptamolybdate (AHM, Sigma-Aldrich) was used as the Mo precursor. For converting AHM to MoO<sub>3</sub>, 0.5 μL droplets were dispensed on one side of each substrate and annealed at 300 °C for 24 min in air. The growth of MoS<sub>2</sub> flakes was done in a three-zone hot-wall furnace with a horizontal cylindrical quartz reactor tube, with 500 sccm Argon serving as carrier gas. In the first zone the carrier gas was enriched with elemental sulfur (Sigma-Aldrich) at a temperature of 170 °C. In the second zone, sulfur reacted with MoO<sub>3</sub> to form MoS<sub>2</sub> monolayers at 750 °C. After the process, the furnace door was opened for cooling.

With an optical microscope, suitable flakes were selected for further processing. Through a standard photolithography process, 10 nm of Cr and 100 nm of Au contacts were deposited by electron-beam (Cr) and thermal evaporation (Au). The lift-off process is done by a 15 min long 80 °C acetone bath, which includes the treatment with ultrasound for one minute, removing excess photoresist with Cr and Au. After the sample is rinsed with acetone, and ethanol.

The samples are placed 3 × 4 h in acetone at 50 °C bath while stirring constantly. The acetone is refreshed each time and rinsed with ethanol. All chemicals used are of analytic quality.

The dried substrates were then glued with silver conductive paint onto a customized sample plate and bonded. The sample plates enable the gating of the sample through a metal surface and simplify the connection for electrical measurements.

### 4.2 PL and Raman Measurements

PL and Raman measurements shown were conducted with a Witec Alpha300 RA setup using a 532 nm cw laser at 1 mW and a 50x (NA 0.55) objective from Zeiss. For PL measurements a grating of 300 lines/mm and for Raman measurements a grating of 1800 lines/mm was used.

### 4.3 AFM

All AFM measurements are done with the Witec Alpha300 RA setup in digital pulsed force mode. The resolution varies between 700 and 1090 pixels/μm<sup>2</sup>. The setpoint was kept at 1.75 V and P gain and L gain at 4 % and 3 %. The driving frequency is 1000 Hz. For all measurements standard force modulation AFM probes by NanoWorld were used.

### 4.4 XPS

XPS measurements were performed on a VersaProbe II by Ulvac-Phi using a monochromatic Al-α,  $\nu = 1486.7$  eV, beam, a beam diameter of 50 μm and an angle between sample surface and analyzer of 45°. To avoid charging of the surface a dual beam charge compensation scheme was applied consisting of electrons and low energy Ar<sup>+</sup> ions.

### 4.5 Electrical Characterization

For electrical and photo-dependent measurements, contacted MoS<sub>2</sub> samples placed in a custom-built vacuum chamber. Measurements were conducted through electric feedthroughs with a two-channel Keithley 2612B source meter. All measurements were done under vacuum conditions ( $\leq 5.5 \times 10^{-5}$  mbar). For photodependent measurements, the channel was illuminated with a 532 nm laser at 0.1 mW laser power focused through a 10x objective from Zeiss (NA 0.25).

## 4.6 Ion Irradiation

Ion irradiation followed a standard protocol [30]. An ion sputtering gun IG35/IG70 from OCI Vacuum Microengineering Inc. was used. Argon gas (99.999% purity; Air Liquide) was filled into the chamber, with a base pressure of  $p_{\text{base}} \approx 1 \times 10^{-8}$  mbar, until a pressure of  $5 \times 10^{-7}$  mbar was reached. A Wien filter for mass separation is employed. The ion current was calibrated to be  $0.36 \mu\text{A}/\text{cm}^2$ . The devices were exposed to the beam until the desired fluence was reached.

## 4.7 DFT Calculations

Spin-polarized electronic structure calculations were performed using Density Functional Theory (DFT) with VASP 6.4.2 version package [58, 59]. The interactions between ions and valence electrons were described using the projector-augmented wave (PAW)[60] method, and electronic exchange and correlation were treated by the generalized gradient approximation of Perdew, Burke, and Ernzerhof (PBE)[61]. The monolayer MoS<sub>2</sub> models were constructed in a  $5 \times 5$  supercell. We employed a plane wave cut-off energy of 500 eV and an additional correction to the van der Waals dispersion interaction in the form of D3 according to Grimme *et al.* [62], employing a Becke-Johnson damping function. 25 Å of vacuum was applied to avoid interaction with the periodic images. A  $2 \times 2 \times 1$  Monkhorst-Pack k-point grid was used to sample the 2D Brillouin zone. The structures were relaxed with PBE until the energy was less than 0.01 eV/Å while the self-consistent convergence limit was  $10^{-6}$  eV. The unfolded band structure was plotted using the assistance of the VASPKIT code [63]. The chemical potentials ( $\mu_i$ ) used to determine the defect formation energies were referenced to their respective elemental reservoirs. Specifically, bulk Mo, bulk S, and graphite (C) were utilized as solid reservoirs, with their reference energies defined as the total energy of the bulk supercell divided by the number of constituent atoms in that supercell. For hydrogen, an isolated gaseous H<sub>2</sub> molecule was employed as the chemical potential reservoir.

## Author Contributions

L.D., S.S., and M.S. and jointly conceived the idea of the study. L.D., under the supervision of M.S., designed the experimental research strategy, wrote the main content of the manuscript, conducted ion irradiation, conducted the electrical characterization, conducted Raman and PL measurements, and performed the associated data analysis. D.S., supervised by P.K., performed all theoretical calculations and co-wrote the manuscript. L.K., supervised by M.S., assisted with measurements and data analysis. O.K., supervised by M.S., synthesized and processed all samples. U.H. performed XPS measurements and the associated data analysis. O.A. performed AFM measurements. L.B. designed the electrical characterization setup. All authors contributed to the interpretation of the results and to the preparation of the manuscript. M.S. supervised the overall project.

## Acknowledgments

The authors gratefully acknowledge financial support from the DFG within the IRTG 2803: 2D Mature, project No. 461605777 and project No. 429784087. Additionally, the authors acknowledge the computing time granted by the Center for Computational Sciences and Simulation (CCSS) of the Universität of Duisburg-Essen and provided on the supercomputer amplitUDE (DFG project 459398823; grant ID INST 20876/423-1 FUGG) at the Zentrum für Informations- und Mediendienste (ZIM). The authors acknowledge support by technical staff, especially Anke Hierzenberger, and helpful discussions with Bruno Schuler.

## Financial disclosure

None reported.

## Conflict of interest

The authors declare no potential conflict of interests.

## Data Availability

The data that support the findings of this study will be openly available following an embargo at the following DOI: 10.17172/nomad.rs84-nxz5

## References

- [1] Ming-Yen Lu, Shang-Chi Wu, Hsiang-Chen Wang, and Ming-Pei Lu. Time-evolution of the electrical characteristics of MoS<sub>2</sub> field-effect transistors after electron beam irradiation. *Phys. Chem. Chem. Phys.*, 20(14):9038–9044, 2018.
- [2] Aniello Pelella, Osamah Kharsah, Alessandro Grillo, Francesca Urban, Maurizio Passacantando, Filippo Giubileo, Laura Lemmo, Stephan Sleziona, Erik Pollmann, Lukas Madauß, Marika Schleberger, and Antonio Di Bartolomeo. Electron irradiation of metal contacts in monolayer MoS<sub>2</sub> field-effect transistors. *ACS Appl. Mater. Interfaces*, 12(36):40532–40540, 2020.
- [3] Stephan Sleziona, Aniello Pelella, Enver Faella, Osamah Kharsah, Lucia Skopinski, André Maas, Yossarian Liebsch, Jennifer Schmeink, Antonio Di Bartolomeo, and Marika Schleberger. Manipulation of the electrical and memory properties of MoS<sub>2</sub> field-effect transistors by highly charged ion irradiation. *Nanoscale Adv.*, 5(24):6958–6966, 2023.
- [4] Simone Bertolazzi, Sara Bonacchi, Guangjun Nan, Anton Pershin, David Beljonne, and Paolo Samorì. Engineering chemically active defects in monolayer MoS<sub>2</sub> transistors via ion-beam irradiation and their healing via vapor deposition of alkanethiols. *Adv. Mater.*, 29(18):1606760, 2017.
- [5] Jakub Jadwiszczak, Darragh Keane, Pierce Maguire, Conor P. Cullen, Yangbo Zhou, Huading Song, Clive Downing, Daniel Fox, Niall McEvoy, Rui Zhu, Jun Xu, Georg S. Duesberg, Zhi-Min Liao, John J. Boland, and Hongzhou Zhang. MoS<sub>2</sub> memtransistors fabricated by localized helium ion beam irradiation. *ACS Nano*, 13(12):14262–14273, 2019.
- [6] Xiaomin Zhang, Jiahan Xu, Aomiao Zhi, Jian Wang, Yue Wang, Wenkai Zhu, Xingjie Han, Xuezheng Tian, Xuedong Bai, Baoquan Sun, Zhongming Wei, Jing Zhang, and Kaiyou Wang. Low-defect-density monolayer MoS<sub>2</sub> wafer by oxygen-assisted growth-repair strategy. *Adv. Sci.*, 11(42):e2408640, 2024.
- [7] Antonio Di Bartolomeo, Luca Genovese, Tobias Foller, Filippo Giubileo, Giuseppe Luongo, Luca Croin, Shi-Jun Liang, L. K. Ang, and Marika Schleberger. Electrical transport and persistent photoconductivity in monolayer MoS<sub>2</sub> phototransistors. *Nanotechnology*, 28(21):214002, 2017.
- [8] Zahra Fekri, Phanish Chava, Gregor Hlawacek, Mahdi Ghorbani-Asl, Silvan Kretschmer, Wajid Awan, Vivek Mootheri, Tommaso Venanzi, Natalia Sycheva, Antony George, Andrey Turchanin, Kenji Watanabe, Takashi Taniguchi, Manfred Helm, Arkady V. Krasheninnikov, and Artur Erbe. Tuning the electronic characteristics of monolayer MoS<sub>2</sub>-based transistors by ion irradiation: The role of the substrate. *Adv. Electron. Mater.*, 10(9):2400037, 2024.
- [9] Kin Fai Mak, Changgu Lee, James Hone, Jie Shan, and Tony F. Heinz. Atomically thin MoS<sub>2</sub>: a new direct-gap semiconductor. *Phys. Rev. Lett.*, 105(13):136805, 2010.
- [10] B. Radisavljevic, A. Radenovic, J. Brivio, V. Giacometti, and A. Kis. Single-layer MoS<sub>2</sub> transistors. *Nat. Nanotechnol.*, 6(3):147–150, 2011.
- [11] Oriol Lopez-Sanchez, Dominik Lembke, Metin Kayci, Aleksandra Radenovic, and Andras Kis. Ultrasensitive photodetectors based on monolayer MoS<sub>2</sub>. *Nat. Nanotechnol.*, 8(7):497–501, 2013.
- [12] Antonio Di Bartolomeo, Luca Genovese, Filippo Giubileo, Laura Lemmo, Giuseppe Luongo, Tobias Foller, and Marika Schleberger. Hysteresis in the transfer characteristics of MoS<sub>2</sub> transistors. *2D Mater.*, 5(1):015014, 2018.
- [13] Daniel S. Fox, Yangbo Zhou, Pierce Maguire, Arlene O’Neill, Cormac Ó’Coileáin, Riley Gatensby, Alexey M. Glushenkov, Tao Tao, Georg S. Duesberg, Igor V. Shvets, Mohamed Abid, Mourad Abid, Han-Chun Wu, Ying Chen, Jonathan N. Coleman, John F. Donegan, and Hongzhou Zhang. Nanopatterning and electrical tuning of MoS<sub>2</sub> layers with a subnanometer helium ion beam. *Nano Lett.*, 15(8):5307–5313, 2015.
- [14] Katherine A. Cochrane, Jun-Ho Lee, Christoph Kastl, Jonah B. Haber, Tianyi Zhang, Azimkhan Kozhakhmetov, Joshua A. Robinson, Mauricio Terrones, Jascha Repp, Jeffrey B. Neaton, Alexander Weber-Bargioni, and Bruno Schuler. Spin-dependent vibronic response of a carbon radical ion in two-dimensional WS<sub>2</sub>. *Nat. Commun.*, 12(1):7287, 2021.
- [15] KA Cochrane, T Zhang, A Kozhakhmetov, JH Lee, F Zhang, C Dong, JB Neaton, JA Robinson, M Terrones, A Weber Bargioni, et al. Intentional carbon doping reveals ch as an abundant charged impurity in nominally undoped synthetic WS<sub>2</sub> and WSe<sub>2</sub>. *2D Mater.*, 7(3):031003, 2020.
- [16] Bruno Schuler, Jun-Ho Lee, Christoph Kastl, Katherine A Cochrane, Christopher T Chen, Sivan Refaely-Abramson, Shengjun Yuan, Edo van Veen, Rafael Roldán, Nicholas J Borys, et al. How substitutional point defects in two-dimensional WS<sub>2</sub> induce charge localization, spin-orbit splitting, and strain. *ACS Nano*, 13(9):10520–10534, 2019.

- [17] Sangwook Park, Samira Siahrostami, Joonsuk Park, Amir Hassan Bagherzadeh Mostaghimi, Taeho Roy Kim, Lauren Vallez, Thomas Mark Gill, Woosung Park, Kenneth E Goodson, Robert Sinclair, et al. Effect of adventitious carbon on pit formation of monolayer MoS<sub>2</sub>. *Adv. Mater.*, 32(37):2003020, 2020.
- [18] Fu Zhang, Yanfu Lu, Daniel S Schulman, Tianyi Zhang, Kazunori Fujisawa, Zhong Lin, Yu Lei, Ana Laura Elias, Saptarshi Das, Susan B Sinnott, et al. Carbon doping of WS<sub>2</sub> monolayers: Bandgap reduction and p-type doping transport. *Sci. Adv.*, 5(5):eaav5003, 2019.
- [19] Youngsin Park, Nannan Li, Daesung Jung, Laishram Tomba Singh, Jaeyoon Baik, Eunsook Lee, Dongseok Oh, Young Dok Kim, Jin Yong Lee, Jeongseok Woo, Seungmin Park, Hanchul Kim, Geunseop Lee, Geunsik Lee, and Chan-Cuk Hwang. Unveiling the origin of n-type doping of natural MoS<sub>2</sub>: carbon. *npj 2D Mater. Appl.*, 7(1):1–7, 2023.
- [20] Lei Liu, Yushu Wang, Ruikang Dong, Dongxu Fan, Si Meng, Lang Wu, Shengqiang Wu, Wei Xu, Mingwei Feng, Ningmu Zou, Qingyu Yan, Zehua Hu, Fei Lu, Shitong Zhu, Yuan Gao, Liang Ma, Yi Shi, Taotao Li, Jinlan Wang, and Xinran Wang. Kinetic acceleration of MoS<sub>2</sub> growth by oxy-metal-organic chemical vapor deposition. *Science*, 391(6784):494–498, 2026.
- [21] Nils Scheuschner, Oliver Ochedowski, Anne-Marie Kaulitz, Roland Gillen, Marika Schleberger, and Janina Maultzsch. Photoluminescence of freestanding single- and few-layer MoS<sub>2</sub>. *Phys. Rev. B*, 89(12):125406, 2014.
- [22] Erik Pollmann, Lukas Madauß, Simon Schumacher, Uttam Kumar, Flemming Heuvel, Christina vom Ende, Sümeyra Yılmaz, Sümeyra Güngörmüş, and Marika Schleberger. Apparent differences between single layer molybdenum disulphide fabricated via chemical vapour deposition and exfoliation. *Nanotechnology*, 31(50):505604, 2020.
- [23] Jason W. Christopher, Bennett B. Goldberg, and Anna K. Swan. Long tailed trions in monolayer MoS<sub>2</sub>: Temperature dependent asymmetry and resulting red-shift of trion photoluminescence spectra. *Sci. Rep.*, 7(1):14062, 2017.
- [24] B. Luo, J. Liu, S. C. Zhu, and L. Yi. Chromium is proposed as an ideal metal to form contacts with monolayer MoS<sub>2</sub> and WS<sub>2</sub>. *Mater. Res. Express*, 2(10):106501, 2015.
- [25] Hui Yang, Sa Cai, Yifei Zhang, Dongping Wu, and Xiaosheng Fang. Enhanced electrical properties of lithography-free fabricated MoS<sub>2</sub> field effect transistors with chromium contacts. *J. Phys. Chem. Lett.*, 12(11):2705–2711, 2021.
- [26] Alessandro Grillo and Antonio Di Bartolomeo. A current-voltage model for double schottky barrier devices. *Adv. Electron. Mater.*, 7(2):2000979, 2021.
- [27] Daniel S. Schulman, Andrew J. Arnold, and Saptarshi Das. Contact engineering for 2D materials and devices. *Chem. Soc. Rev.*, 47(9):3037–3058, 2018.
- [28] Sujay B. Desai, Surabhi R. Madhvapathy, Angada B. Sachid, Juan Pablo Llinas, Qingxiao Wang, Geun Ho Ahn, Gregory Pitner, Moon J. Kim, Jeffrey Bokor, Chenming Hu, H-S Philip Wong, and Ali Javey. MoS<sub>2</sub> transistors with 1-nanometer gate lengths. *Science*, 354(6308):99–102, 2016.
- [29] Arun Kumar, Enver Faella, Ofelia Durante, Filippo Giubileo, Aniello Pelella, Loredana Viscardi, Kimberly Intonti, Stephan Sleziona, Marika Schleberger, and Antonio Di Bartolomeo. Optoelectronic memory in 2D MoS<sub>2</sub> field effect transistor. *J. Phys. Chem. Solids*, 179:111406, 2023.
- [30] Ruofei Zheng, Leon Daniel, Dedi Sutarma, Christian Viernes, Yingfang Ding, Tobiloba Fabunmi, Gerd Bacher, Michael Heuken, Holger Kalisch, Andrei Vescan, Peter Kratzer, Marika Schleberger, and Germán Sciaini. Defect-engineered competition between exciton annihilation and trapping in MOCVD WS<sub>2</sub>. *Chem. Sci.*, 17(2):1176–1185, 2026.
- [31] Lesheng Li and Emily A. Carter. Defect-mediated charge-carrier trapping and nonradiative recombination in WSe<sub>2</sub> monolayers. *J. Am. Chem. Soc.*, 141(26):10451–10461, 2019.
- [32] Long Yuan and Libai Huang. Exciton dynamics and annihilation in WS<sub>2</sub> 2D semiconductors. *Nanoscale*, 7(16):7402–7408, 2015.
- [33] Muhammad Shamim Al Mamun, Yasuyuki Sainoo, Tsuyoshi Takaoka, Atsushi Ando, and Tadahiro Komeda. Hysteresis in the transfer characteristics of MoS<sub>2</sub> field effect transistors: gas, temperature and photo-irradiation effect. *RSC Adv.*, 14(49):36517–36526, 2024.
- [34] Matteo Farronato, Piergiulio Mannocci, Margherita Melegari, Saverio Ricci, Christian Monzio Compagnoni, and Daniele Ielmini. Reservoir computing with charge-trap memory based on a MoS<sub>2</sub> channel for neuromorphic engineering. *Adv. Mater.*, 35(37):e2205381, 2023.

- [35] Yury Yu Illarionov, Theresia Knobloch, Markus Jech, Mario Lanza, Deji Akinwande, Mikhail I. Vexler, Thomas Mueller, Max C. Lemme, Gianluca Fiori, Frank Schwierz, and Tibor Grasser. Insulators for 2D nanoelectronics: the gap to bridge. *Nat. Commun.*, 11(1):3385, 2020.
- [36] Yury Yu Illarionov, Theresia Knobloch, Michael Waltl, Gerhard Rzepa, Andreas Pospischil, Dmitry K. Polyushkin, Marco M. Furchi, Thomas Mueller, and Tibor Grasser. Energetic mapping of oxide traps in MoS<sub>2</sub> field-effect transistors. *2D Mater.*, 4(2):025108, 2017.
- [37] Bernhard Stampfer, Feng Zhang, Yury Yuryevich Illarionov, Theresia Knobloch, Peng Wu, Michael Waltl, Alexander Grill, Joerg Appenzeller, and Tibor Grasser. Characterization of single defects in ultrascaled MoS<sub>2</sub> field-effect transistors. *ACS Nano*, 12(6):5368–5375, 2018.
- [38] Amina Zafar, Haiyan Nan, Zainab Zafar, Zhangting Wu, Jie Jiang, Yumeng You, and Zhenhua Ni. Probing the intrinsic optical quality of CVD grown MoS<sub>2</sub>. *Nano Res.*, 10(5):1608–1617, 2017.
- [39] Yakui Mu, Siyu Liu, Yanming Wang, Chen Shu, Yi Han, Kai Liu, Zengqin Song, Yang Wang, Xiaoyan Yan, Zhikun Liu, and Mingzhen Zhao. Mobility enhancement in monolayer MoS<sub>2</sub> transistors on a polyimide substrate by reducing localized charge trap effect. *ACS Appl. Electron. Mater.*, 7(18):8571–8582, 2025.
- [40] Wenjuan Zhu, Tony Low, Yi-Hsien Lee, Han Wang, Damon B. Farmer, Jing Kong, Fengnian Xia, and Phaedon Avouris. Electronic transport and device prospects of monolayer molybdenum disulphide grown by chemical vapour deposition. *Nat. Commun.*, 5(1):3087, 2014.
- [41] Yakui Mu, Siyu Liu, Yanming Wang, Zhikun Liu, and Mingzhen Zhao. Understanding electron transport mechanisms in monolayer MoS<sub>2</sub> transistors: Impact of lattice phonon scattering and localized charge traps. *Phys. Rev. B*, 110(11), 2024.
- [42] Zhihao Yu, Zhun-Yong Ong, Songlin Li, Jian-Bin Xu, Gang Zhang, Yong-Wei Zhang, Yi Shi, and Xinran Wang. Analyzing the carrier mobility in transition-metal dichalcogenide MoS<sub>2</sub> field-effect transistors. *Adv. Funct. Mater.*, 27(19):1604093, 2017.
- [43] Zhihao Yu, Zhun-Yong Ong, Yiming Pan, Yang Cui, Run Xin, Yi Shi, Baigeng Wang, Yun Wu, Tangsheng Chen, Yong-Wei Zhang, Gang Zhang, and Xinran Wang. Realization of room-temperature phonon-limited carrier transport in monolayer MoS<sub>2</sub> by dielectric and carrier screening. *Adv. Mater.*, 28(3):547–552, 2016.
- [44] Song-Lin Li, Katsunori Wakabayashi, Yong Xu, Shu Nakaharai, Katsuyoshi Komatsu, Wen-Wu Li, Yen-Fu Lin, Alex Aparecido-Ferreira, and Kazuhito Tsukagoshi. Thickness-dependent interfacial coulomb scattering in atomically thin field-effect transistors. *Nano Lett.*, 13(8):3546–3552, 2013.
- [45] Marco M. Furchi, Dmitry K. Polyushkin, Andreas Pospischil, and Thomas Mueller. Mechanisms of photoconductivity in atomically thin MoS<sub>2</sub>. *Nano Lett.*, 14(11):6165–6170, 2014.
- [46] Andreij C. Gadelha, Alisson R. Cadore, Lucas Lafeta, Ana M. de Paula, Leandro M. Malard, Rodrigo G. Lacerda, and Leonardo C. Campos. Local photodoping in monolayer MoS<sub>2</sub>. *Nanotechnology*, 31(25):255701, 2020.
- [47] Silvan Kretschmer, Mikhail Maslov, Sadegh Ghaderzadeh, Mahdi Ghorbani-Asl, Gregor Hlawacek, and Arkady V. Krasheninnikov. Supported two-dimensional materials under ion irradiation: The substrate governs defect production. *ACS Appl. Mater. Interfaces*, 10(36):30827–30836, 2018.
- [48] James F. Ziegler, M. D. Ziegler, and J. P. Biersack. SRIM – the stopping and range of ions in matter (2010). *Nucl. Instrum. Methods Phys. Res. B: Beam Interact. Mater. At.*, 268(11-12):1818–1823, 2010.
- [49] Mahdi Ghorbani-Asl, Silvan Kretschmer, Douglas E. Spearot, and Arkady V. Krasheninnikov. Two-dimensional MoS<sub>2</sub> under ion irradiation: from controlled defect production to electronic structure engineering. *2D Mater.*, 4(2):025078, 2017.
- [50] Arkady V. Krasheninnikov, Matthias Batzill, Anouar-Akacha Delenda, Marija Drndić, Chris Ewels, Katharina J. Franke, Mahdi Ghorbani-Asl, Alexander Holleitner, Ado Jorio, Ute Kaiser, Daria Kieczka, Hannu-Pekka Komsa, Jani Kotakoski, Manuel Längle, David Lamprecht, Yun Liu, Steven G. Louie, Janina Maultzsch, Thomas Michely, Katherine Milton, Anna Niggas, Hanako Okuno, Joshua A. Robinson, Marika Schleberger, Bruno Schuler, Alexander Shluger, Kazu Suenaga, Kristian S. Thygesen, Richard A. Wilhelm, E. Harriet Åhlgren, and Carla Bittencourt. Defects and defect-mediated engineering of two-dimensional materials: challenges and open questions. *Beilstein J. Nanotechnol.*, 17(1):454–488, 2026.
- [51] Stephan Sleziona, Osamah Kharsah, Lucia Skopinski, Leon Daniel, Jennifer Schmeink, and Marika Schleberger. Influence of highly charged ion irradiation on the electrical and memory properties of black phosphorus field-effect transistors. *Adv. Electron. Mater.*, 11(2):2400318, 2025.
- [52] Leon Daniel, Dedi Sutarma, Osamah Kharsah, Charleen Lintz, Henrik Myja, Peter Kratzer, and Marika Schleberger. Mechanism of oleic acid-mediated sulfur vacancy healing in monolayer WS<sub>2</sub>. *ACS Nanosci. Au*, 5(6):576–584, 2025.

- [53] Lisa Frammolino, Madisen Holbrook, Chao Lei, Jeng-Yuan Tsai, Yi Wan, Lin-Yun Huang, Lain-Jong Li, Qimin Yan, Allan MacDonald, and Chih-Kang Shih. Microscopic investigations of point defect interactions in WS<sub>2</sub> monolayers. *ACS Nano*, 19(37):33059–33069, 2025.
- [54] Aiqing Wu, Qinggong Song, and Hongpeng Liu. Oxygen atom adsorbed on the sulphur vacancy of monolayer MoS<sub>2</sub>: A promising method for the passivation of the vacancy defect. *Comput. Theor. Chem.*, 1187:112906, 2020.
- [55] Ziyu Luo, Weihao Zheng, Nannan Luo, Bo Liu, Biyuan Zheng, Xing Yang, Delang Liang, Junyu Qu, Huawei Liu, Ying Chen, Ying Jiang, Shula Chen, Xiaolong Zou, and Anlian Pan. Photoluminescence lightening: Extraordinary oxygen modulated dynamics in WS<sub>2</sub> monolayers. *Nano Lett.*, 22(5):2112–2119, 2022.
- [56] András Pálinkás, György Kálvin, Péter Vancsó, Konrád Kandrai, Márton Szendrő, Gergely Németh, Miklós Németh, Áron Pekker, József S. Pap, Péter Petrik, Katalin Kamarás, Levente Tapasztó, and Péter Nemes-Incze. The composition and structure of the ubiquitous hydrocarbon contamination on van der waals materials. *Nat. Commun.*, 13(1):6770, 2022.
- [57] Erik S. Cheng and Gyeong S. Hwang. Low-energy argon ion bombardment-induced decomposition of physisorbed hydrofluorocarbons on silicon nitride surfaces: A computational mechanistic study. *J. Chem. Phys.*, 159(1), 2023.
- [58] G. Kresse and D. Joubert. From ultrasoft pseudopotentials to the projector augmented-wave method. *Phys. Rev. B*, 59(3):1758–1775, 1999.
- [59] G. Kresse and J. Furthmuller. Efficient iterative schemes for ab initio total-energy calculations using a plane-wave basis set. *Phys. Rev. B*, 54(16):11169–11186, 1996.
- [60] P. E. Blochl. Projector augmented-wave method. *Phys. Rev. B*, 50(24):17953–17979, 1994.
- [61] J. P. Perdew, K. Burke, and M. Ernzerhof. Generalized gradient approximation made simple. *Phys. Rev. Lett.*, 77(18):3865–3868, 1996.
- [62] Stefan Grimme, Stephan Ehrlich, and Lars Goerigk. Effect of the damping function in dispersion corrected density functional theory. *J. Comput. Chem.*, 32(7):1456–1465, 2011.
- [63] Vei Wang, Nan Xu, Jin-Cheng Liu, Gang Tang, and Wen-Tong Geng. Vaspkit: A user-friendly interface facilitating high-throughput computing and analysis using vasp code. *Comput. Phys. Commun.*, 267:108033, 2021.